applied sciences

MDPI

Article

Parallel Load-Bearing and Damping System Design and Test for Satellite Vibration Suppression

Shenyan Chen [1,*], Zihan Yang [1], Minxiao Ying [1], Yanwu Zheng [1], Yanjie Liu [1] and Zhongwen Pan [2]

[1] School of Astronautics, Beihang University, Beijing 100191, China; yangzihan@buaa.edu.cn (Z.Y.); yingminxiao@buaa.edu.cn (M.Y.); buaa_zyw@buaa.edu.cn (Y.Z.); zy1415135@buaa.edu.cn (Y.L.)

[2] Beijing Institute of Aerospace System Engineering, Beijing 100076, China; zhwpan@sina.com

* Correspondence: chenshenyan@buaa.edu.cn

Received: 31 December 2019; Accepted: 16 February 2020; Published: 24 February 2020

Abstract: The traditional series-type satellite vibration suppression scheme significantly decreases satellite frequency, which leads to difficulty in controlling the amplitude. In the present work, a new parallel viscous damping scheme is adopted on the Payload Adaptor Fitting (PAF), which aims to integrate a load-bearing design and vibration reduction. The vibration amplitude and weight are the most important design requirements of the damping system. The Finite Element (FE) model of PAF was established. Through a series of analyses, the appropriate number and coefficient of dampers were determined. The damping force was calculated according to the damping coefficient and the relative velocity between the two ends of the damper. Based on the damping force and the installation dimensions, the damping rod was designed. The force–velocity test was carried out on the damping rod prototype, which showed its performance satisfies the requirements. With the topology optimization and sizing optimization technology, the light-weight supports were designed and manufactured. One damping rod and two supports were assembled as one set of dampers. Eight sets of dampers were installed on the PAF. Vibration tests were conducted on the damping state PAF. The results showed that the proposed system is effective at suppressing vibration and maintaining stiffness simultaneously.

Keywords: parallel vibration reduction; viscous damper; damping system design

1. Introduction

Satellites are subjected to a complex vibration environment during launch [1]. Vibrations are transmitted through the interface of the rocket and the satellite, which includes high-frequency and low-frequency vibrations. The high-frequency random vibration is mainly produced by noise excitation [2,3]. The low-frequency vibration is generally under 100 Hz, which is mainly caused by two sources: (1) the free vibration decay from the transient excitations, such as the rocket engine's ignition/shutdown, the inter-stage separations, and the booster separations; and (2) unstable vibrations from the intercoupling between the liquid rocket propulsion system and the structure system [4,5].

The fundamental frequency of a satellite structure is usually under 100 Hz, which is near the low-frequency vibration environment. Therefore, there is vibration amplification in flight and ground tests, which might cause serious consequences such as structural damage.

In order to protect satellites dynamically in the launch environment, a series-type vibration isolation technology was proposed. CSA Engineering Inc. has been working on the concept of the whole-spacecraft vibration isolation system since 1993 for The Air Force Research Laboratory. Its typical product is SoftRide, which includes Uniflex for axial vibration attenuation [6] and MultiFlex for both axial and lateral vibration attenuation [7]. Later, Sciulli improved the CSA passive system by using

active components to adapt to the dynamic environment during the launch with both broadband and narrowband attenuation [8]. Ruebsamen developed the EVLIS (Evolved Launch Vibration Isolation System) prototype, implementing integrated active and passive vibration control [9]. Yang et al. proposed whole-spacecraft disk vibration isolators based on a reliability method, which have a great impact on medium-high frequency [10]. Stabile designed a negative resistance electromagnetic shunt damper aimed at the micro vibration [11]. Zhanji W. advanced a method using a metal robber damping rod, which isolates high-frequency vibration as well as restraining the resonant peak effectively [12]. Shaochong established some principles for the vibration isolation design, and they could be adopted to restrain the resonance and isolate the response in a higher frequency domain [13]. Gangtie developed an octo-strut vibration isolation platform based on the Stewart platform and improved the reliability and load capacity of the original platform [14]. Yao Z. designed a vibration isolation system with magnetic suspension, which can provide a greater restoring force for better dynamic performance [15]. Changcheng added a metal-rubber shock absorber on the satellite to improve the space camera's image quality [16]. Yewei showed that the dynamic features are not affected by the stiffness of viscoelastic material of the vibration control system [17].

However, the principle of traditional series-type whole-spacecraft vibration isolation is changing the frequency and reducing the amplitude. As a result, in practical engineering problems, the satellite branch frequency significantly decreases after introducing the vibration isolation system. This leads to the instability of the attitude. To solve this problem, Du came up with a new scheme. Constrained damping layers are attached to the main load-carrying structure like the payload adapter. With this scheme, the damping of the whole structure increases, while the stiffness is maintained [18,19]. Jiaxiong also adopted a constrained damping layer on a spacecraft instrument installation board [20]. Tu studied semi-active vibration isolation technology, making use of the high reliability of magnetorheological damper [21]. The two schemes adopt the concept of a parallel system, which has good performance on vibration suppression.

Based on previous research, this article presents the design of a parallel damping scheme for a satellite's vibration isolation. This scheme connects viscous dampers in parallel with a specific structure: Payload Adaptor Fitting (PAF). The FE model of the PAF with the damping system was analyzed to design the damping rod. Topology and sizing optimization technology is used for the light-weight support design. Vibration experiments were conducted to verify the effectiveness of the damping system. The experiments were performed by Zhongwen [22]. The results prove that the new system can reduce the vibration response and achieve the integration of load bearing and vibration isolation, as well as maintaining the PAF's stiffness.

2. Problem Description

The whole-spacecraft vibration isolation system, which is shown in Figure 1, attenuates the vibration load that is transmitted from the launch vehicle to the payload. Payload Adaptor Fitting (PAF) is the section connecting the launch vehicle with the satellite and is traditionally designed to be very stiff and provide an efficient transmission path for both dynamic and quasi-static launch loads [23]. The satellite branch structure consists of a satellite and a Payload Adaptor Fitting (PAF), which is shown in Figure 2. In engineering problems, there is a satellite holder connecting the satellite on the top of the PAF, and a rocket connector is at the bottom of the PAF.

In order to characterize and analyze the dynamic properties of the PAF, an experiment was conducted to get its frequency response. In the experiment, the bottom of the PAF was connected to a vibration machine, which could simulate the vibration transmitted from the rocket. The testing frequency range and amplitude were 5–100 Hz and 1 m/s^2, respectively.

The results of the frequency responses are shown in Table 1. The first resonance axial, lateral-y, and lateral-z peak frequencies are listed. Their transfer rates are 14.05 m/s^2, 3.1 m/s^2 and 2.4 m/s^2, respectively. The acceleration peak is so high that a structure would be damaged if no vibration isolation measure was adopted.

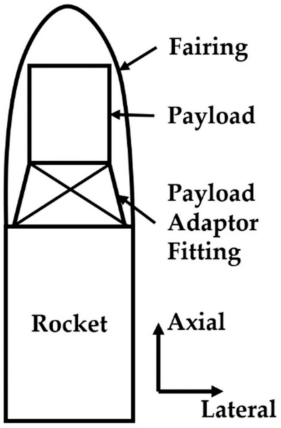

Figure 1. The sketch of the whole-spacecraft vibration isolation system.

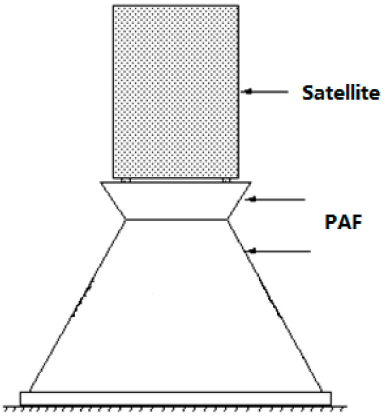

Figure 2. Satellite branch structure.

Table 1. Peak frequencies and acceleration transmissibility.

	Peak Frequency/Hz	Acceleration/(m/s^2)
Axial(X)	28.33	14.05
Lateral(Y)	7.5	3.1
Lateral(Z)	7.5	2.4

Therefore, the overall objective is to reduce the peak value of acceleration transmissibility with the constraint of the fundamental frequency. Because the satellite and rocket's interface cannot be modified, the design object is limited to the PAF. Our goal is to introduce a vibration isolation system on the PAF structure, as well as keep the structure lightweight. In summary, the design requirements are that the axial peak of frequency response at the first order longitudinal frequency reduces to the given level (40% off) and the weight increases by less than 30 kg. In order to maintain structural stability, other design constraints should also be considered: (1) the interface should remain unchanged; (2) the axial and lateral fundamental frequencies should have minimal change.

3. Theoretical Principle

In order to analyze the vibration characteristics of PAF, the satellite branch structure should be simplified. If the satellite is regarded as a rigid body and the PAF is regarded as a spring-damper system, the whole system can be simplified as a Single-Degree-of-Freedom (SDF) system, as demonstrated in Figure 3a. The traditional series-type method changes k or c to suppress vibration.

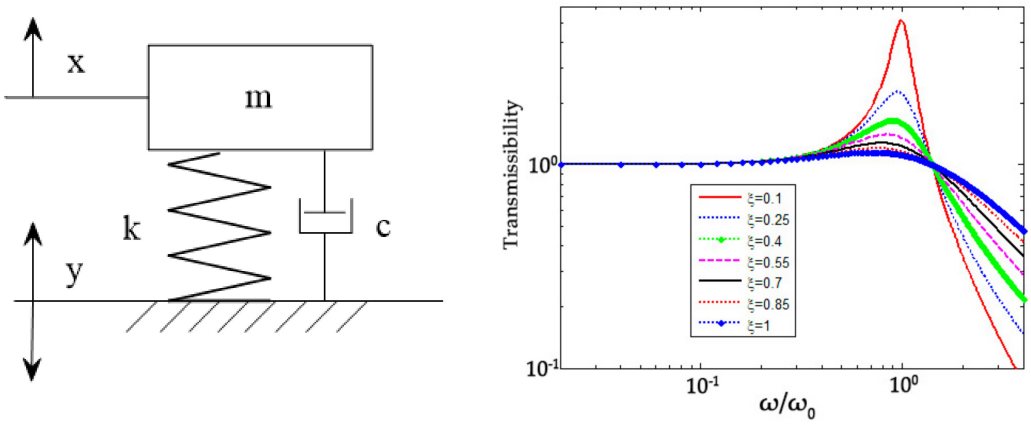

(**a**) (**b**)

Figure 3. Single-Degree-of-Freedom (SDF) system: (**a**) SDF system schematic; (**b**) SDF system transmissibility.

Then, the fundamental frequency would be $\omega_0 = \sqrt{\frac{k}{m}}$, and the damping ratio would be $\xi = \frac{c}{2m\omega_0}$. When increasing the value of c to reduce vibration, ξ would increase as well. As Figure 3b shows, if ω_0 is greater than $\omega/\sqrt{2}$, the transmissibility decreases as the damping ratio ξ increases. On the contrary, if ω_0 is less than $\omega/\sqrt{2}$, the transmissibility increases as ξ increases.

In practical engineering problems, the low-frequency vibration environment is usually under 100 Hz, while the lateral and axial fundamental frequencies of satellites are all under 50 Hz, which is less than $100/\sqrt{2}$ Hz. Therefore, when ξ increases, the transmissibility increases, which is not expected.

In that way, a parallel scheme was adopted for vibration suppression, which can effectively reduce the transmissibility as well as keep the fundamental frequency unchanged. In this scheme, the damping system is parallel to the PAF. The authors of [21] proposed a passive vibration isolation scheme based on the Stewart platform, which is shown in Figure 4. This new scheme is considered a parallel scheme, instead of a series-type scheme. In the present work, this scheme was adopted, and dampers were installed on the PAF for vibration suppression.

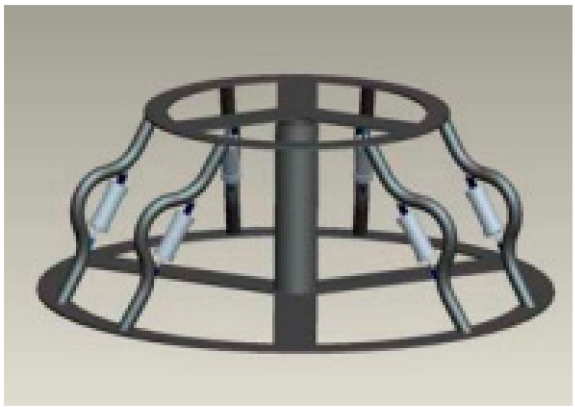

Figure 4. Parallel damping system [21].

4. FE Modeling and Analysis for the Damping System

4.1. FE Modeling for the Damping System

In order to improve the damping effect, dampers were installed on the PAF. The PAF had stringers, skins and four round brackets. With four brackets, the PAF was divided into three parts. Since the dampers could not cross the round brackets, they were installed on the top, middle and bottom parts of the PAF. If dampers are fixed in the top part or the bottom part, they are required to be connected with

the satellite holder or the rocket connecter, which would lead to some limitations, like the dampers' sizes or installation methods. The middle part is the most appropriate for installing dampers. The partial skins between the middle two round brackets were removed to install eight dampers. The dampers were attached to the brackets by hinges, and their element type was a "damper" of 1D. The damping coefficient was assigned. The damping force could be determined by the damping coefficient and the relative velocity between the two ends of the damper. The FE model is shown in Figure 5.

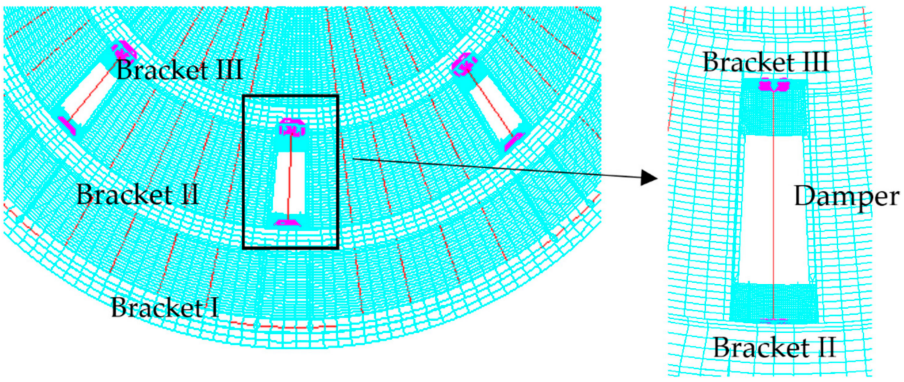

Figure 5. Finite element modeling of the damping system on the Payload Adaptor Fitting (PAF).

4.2. FE Analysis for the Damping System

In order to obtain the appropriate parameters for the damping system, FE analysis was necessary. By changing the number and the damping coefficient of the dampers, five combinations were considered, as shown in Table 2. By comparing these analysis results, the first and fourth results' damping effects were shown to be not good enough. The fifth result's damper number was too large. The best two results were the second and the third. Considering that a higher damping coefficient means higher weight of the structure, which is not expected, result two could fulfill the requirements. The final damping system was composed of eight dampers with the coefficient of 2.8 million N·s/m.

Table 2. Damping coefficient designs and results.

No.	Damping Coefficients (* Number of the Dampers)/(N·s/m)	Axial/(m/s^2)	Lateral/(m/s^2)	Attenuation Percentage	
				Axial	Lateral
/	No dampers	37.7	27.3	/	/
1	700,000 (* 8)	32.5	23.4	13.79%	14.29%
2	2,800,000 (* 8)	22.5	20.1	40.32%	26.37%
3	3,200,000 (* 8)	21.3	20.3	43.50%	25.64%
4	2,800,000 (* 4)	27.8	22.0	26.26%	19.41%
5	1,200,000 (* 16)	22.5	20.1	40.32%	26.37%

In order to confirm that the introduction of the dampers on the PAF will not affect the structure's original characteristics, FE analysis results of the original state and the viscous damping state were compared, as shown in Figure 6. Results of the finite element analysis are shown in Table 3. The skins and stringers affected the structure's transverse bending frequency and longitudinal frequency, respectively. As seen from Table 3, after adding dampers in a viscous damping state, transverse and longitudinal frequencies reduced by less than 0.1 Hz compared with the original model. As a result, the addition of dampers has little effect on the stability of an attitude control system and a fairing's dynamic clearance.

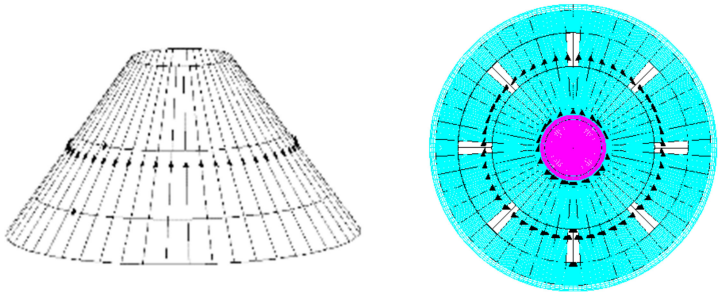

(**a**) (**b**)

Figure 6. PAF model: (**a**) original state; (**b**) viscous damping state.

Table 3. Fundamental frequencies in original state and in viscous damping state.

Fundamental Frequency	Original State/Hz	Damping State/Hz
Transverse (I III)	7.91	7.86
Transverse (II IV)	7.96	7.93
Longitudinal	28.56	28.54

As shown in Section 2, the axial peak frequency and acceleration transmissibility of the original state in the experiment were 28.33 Hz and 14.05 m/s^{2,} respectively. Compared with the experiment results, the FEA results were 28.56 Hz and 14.1 m/s^2, respectively. The frequency difference was 0.8%, while the transmissibility difference was 0.4%. The discrepancies could be negligible, considering the error factors.

The removal of the partial skins may affect the strength of the PAF. Therefore, two harsh working conditions were chosen to indicate whether the strengths were within the requirement: (1) the second stage engine shut down; (2) the satellite is in a transonic condition. The material of the model was aluminum alloy 2A14, and the parameters are shown in Table 4. The maximum stresses were 57.9 MPa and 131 MPa, respectively, which are less than the yield stress of material 2A14. The results prove that the PAF would not be damaged after introducing the damping system.

Table 4. Properties of aluminum alloy.

Material	E_1/Gpa	G_{12}/Gpa	υ	ρ/(Kg/m^3)	σ_s/Mpa
2A14	72	27	0.3	2780	360

5. Damping Rod Design and Test

The relative velocity between two ends of the dampers can be obtained from the FEA results. For eight dampers with the coefficient of 2.8 million N·s/m, the max relative velocity is 1.09×10^{-2} m/s. Then, the max damping force could be calculated from the FEA results, which is 31128 N. The damping rod's stroke and the diameter of damping rod should also be considered. Therefore, a suitable damping rod that could satisfy all the requirements was customized. The outer diameter of the damping rod was 90 mm. Its prototype was tested. The force–velocity curve is shown Figure 7. The star in the figure shows the max damping force under the max velocity is a bit higher than the designed value, which means the damping rod could get better damping effectiveness as well as meet design indicators.

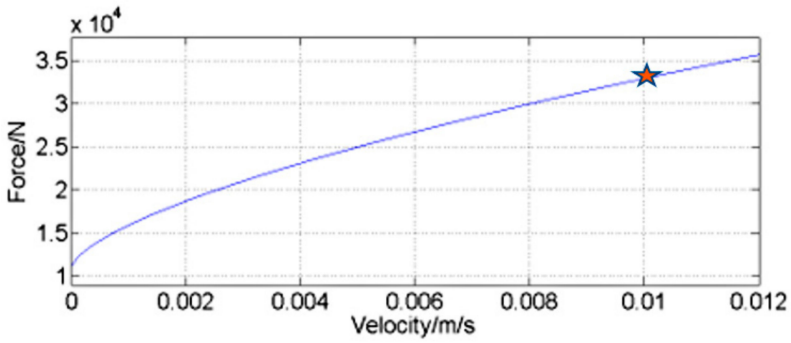

Figure 7. Damping rod's force–velocity curve.

Dampers are generally cylinder-piston type. The damping force is calculated as

$$F = CV^{\alpha},$$

where F is the damping force, V is the velocity of piston rod, C is the damping coefficient, which is related to the cylinder diameter, the piston diameter, the fluid viscosity etc., and α is the velocity exponent based on the structure of the damper. Most dampers are non-linear, which means α does not equal one. The characteristic of a non-linear damper is that the equivalent linear damping coefficient for low speed is larger than that for high speed. This means that the damper can always supply enough damping force even at a low velocity and is not too large to result in structure damage in high velocity. The coefficient–velocity curve of the customized damping rod is shown in Figure 8.

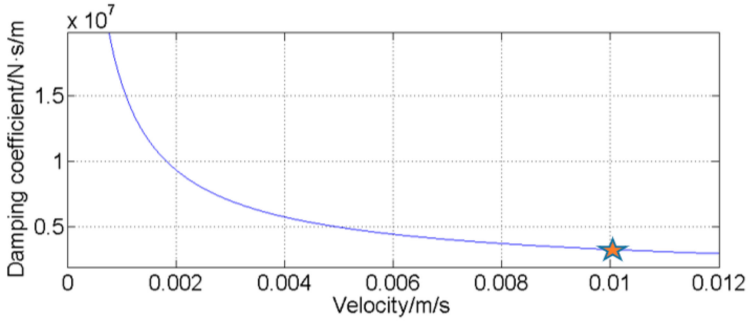

Figure 8. Damping rod's coefficient–velocity curve.

Furthermore, the damper's elastomeric damping material is semi-fluid. This kind of material has a high viscosity and strong compression performance. In addition, it has good chemical stableness, aging resistance, and excellent thermo-stabilization.

6. Lightweight Support Design

To avoid the interference between the dampers and the PAF, supports are necessary. The damping force is transferred through the supports, so they are required to withstand the peak damping force. Because the weight of the dampers' main parts is heavy (3.75 kg × 8 = 30 kg), supports should be as light as possible. In summary, the supports' structure should be designed and optimized according to the PAF's structure and damping force.

As shown in Chapter 5, the max damping force is known to be 31.128 kN. The supports' design load is 32 kN, which is applied on the lugs. Therefore, the boundary condition is that six degrees of freedom of all bolt holes are fixed, and the concentrated force is 32 kN. There are two load cases; the only difference is the direction of the damping force, which can be ±32 kN.

The original designs of upper and lower supports are shown in Figure 9. First, topology optimization was performed by *Altair Inspire* software. With the draw direction constraints, the optimization results were as shown in Figure 10.

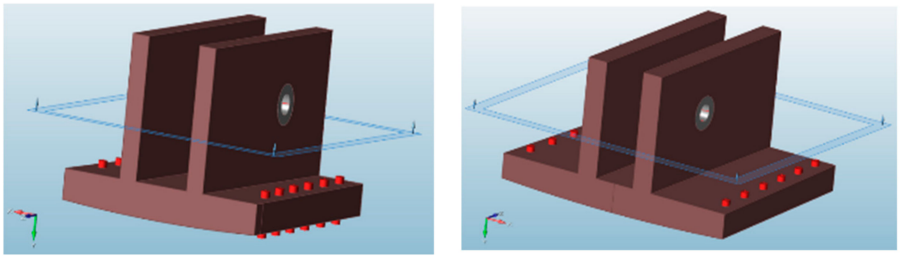

(**a**) (**b**)

Figure 9. Supports' original design: (**a**) upper support; (**b**) lower support.

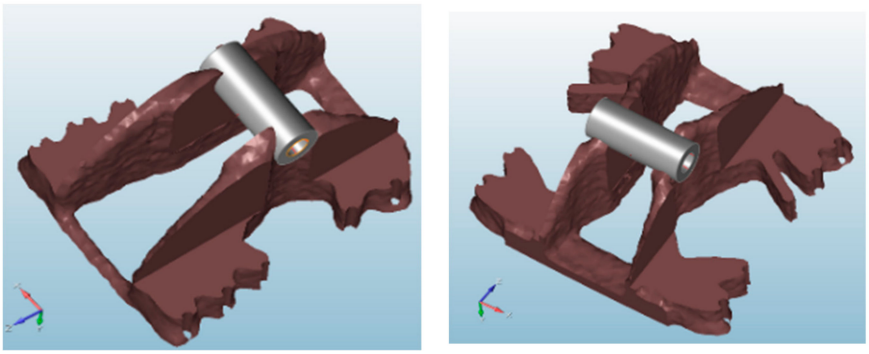

(**a**) (**b**)

Figure 10. Supports' topology optimization results: (**a**) upper support; (**b**) lower support.

According to the topology optimization results, the geometric model was reconstructed by *CATIA*. The middle plane of the earpiece and the base was extracted to build the corresponding FE model, which is shown in Figure 11. This FE model was used to perform sizing optimization. Another engineering constraint is that the thickness of the lugs cannot be less than 8 mm. The sizing optimization problem and results are shown in Table 5**.** The base thicknesses were added, because the strength of the structure near the bolt hole exceeds the stress constraint. The results were rounded for technical requirements.

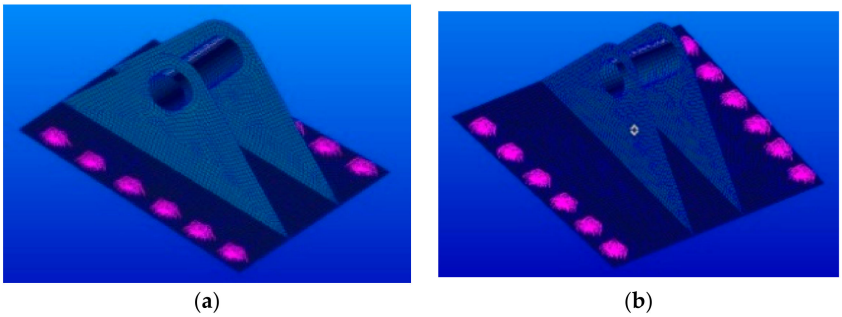

(**a**) (**b**)

Figure 11. Sizing optimization FE model: (**a**) upper support; (**b**) lower support.

After sizing optimization, the following minute adjustments were made. At first, a three-dimensional geometric model was created based on the sizing optimization results. Then, some parts of materials of the model were removed based on the former topology optimization results. To further reduce the supports' weights, some low stress elements were removed according to FE static analysis results. Finally, the weight was controlled to less than 0.5 kg for each support, and the final structures are shown in Figure 12.

Table 5. Sizing optimization model and results.

Object		Weight				
Constraint		Stress < 160 MPa				
Variables		Lower Bound	Upper Bound	Original	Result	Rounded Value
Upper support	Base thickness/mm	1	20	10	15.36	15
	Lugs thickness/mm	1	20	10	7	8
Lower support	Base thickness/mm	1	20	10	15.42	15.5

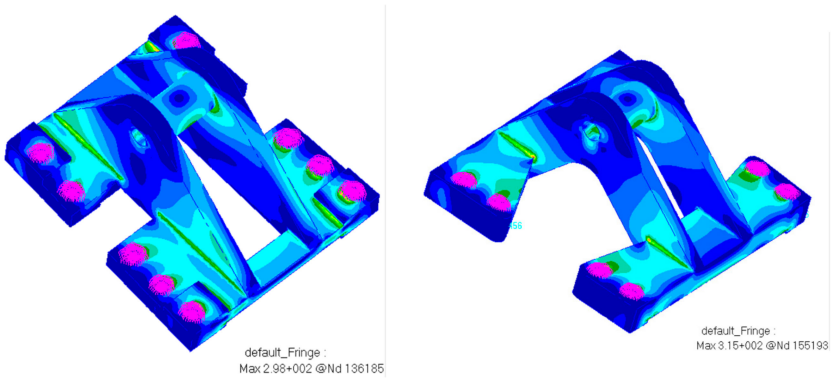

(**a**) (**b**)

Figure 12. Final supports structure: (**a**) upper support; (**b**) lower support.

One damping rod and two supports were assembled as a set of dampers. The structure of the damper is shown in Figure 13a. The assembly model of PAF with the damping system is shown in Figure 13b.

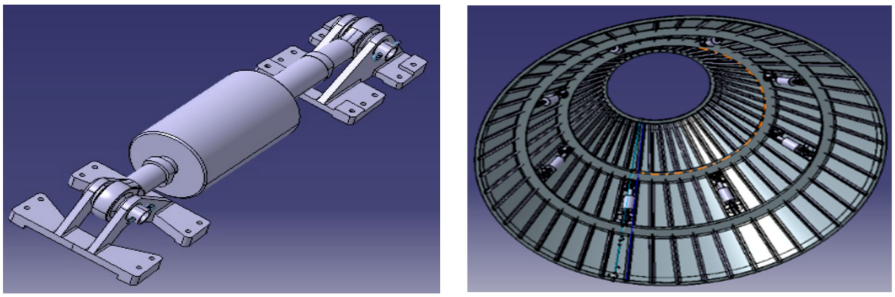

(**a**) (**b**)

Figure 13. Three-dimensional model: (**a**) one set of dampers; (**b**) PAF with the damping system.

7. Experiment Results

After designing the vibration isolation system, frequency response experiments were conducted to verify the effectiveness of the system. By adding dampers, the damping state PAF was manufactured as shown in Figure 14. The bottom of the PAF was connected to a vibration machine as in the original state, to simulate the vibrations transmitted from the rocket. The testing frequency range and amplitude were 5–100 Hz and 1 m/s^{2,} respectively. There were four measuring points that were used to obtain the acceleration characteristics and the vibration transfer properties. The acceleration measuring points were distributed at the four points where the satellite is connected with the PAF. Two measuring points are marked in Figure 14**,** while the other two were at the back of the equipment and are invisible in the figure. The results were averaged over the four measuring points.

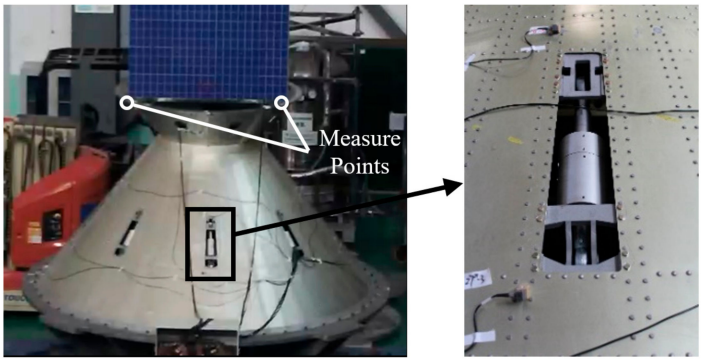

Figure 14. Damping state PAF and the damper.

The frequency response analysis results of the damping state and the original state are shown in Figure 15. The results show that (1) the axial transmissibility of the damping state has obvious attenuation at the first two peaks compared with the original state; (2) the lateral transmissibility has obvious attenuation at the first peak; (3) at other frequency ranges, the transmissibility of the damping state is almost the same as the original.

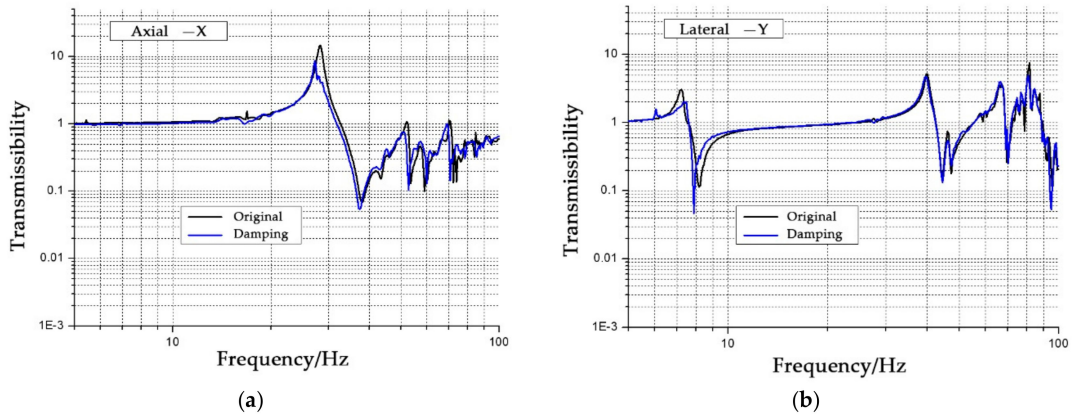

(**a**) (**b**)

Figure 15. Frequency response analysis results: (**a**) axial-X; (**b**) lateral-Y.

To make a better comparison between the damping state and the original state, Table 6 is shown below. The frequency deviation and attenuation percent are reductions of the damping state over the original state. All values in the table are rounded. From the table, it can be seen that the transmissibility of the axial acceleration peak decreased by 35.9%, and the transmissibility of the lateral (y) and lateral (z) acceleration peaks decreased by 34.6% and 12.5%, respectively. The fundamental frequency deviation was less than 5%. This indicates that the transverse and longitudinal stiffnesses were basically unchanged, ensuring the stability of the attitude control system and the safety of the dynamic clearance of the fairing.

Table 6. Comparison of peak frequency and acceleration transmissibility between the original state and damping state.

	Original State		Damping State		Frequency Deviation	Attenuation Percent
	Frequency/Hz	Acceleration	Frequency/Hz	Acceleration		
Axial (X)	28.33	14.05	27.28	9.00	3.7%	35.9%
Lateral (Y)	7.5	3.1	7.2	2.0	3.5%	34.6%
Lateral (Z)	7.5	2.4	7.2	2.1	4.4%	12.5%

8. Conclusions

In the present work, a parallel damping vibration suppression scheme was adopted to improve the spacecraft interface's complex vibration environment, which could simultaneously maintain the structural stiffness. The number and coefficient of dampers were designed by comparison of the frequency response analysis results. As a result, the PAF was mounted with eight dampers. Based on the new model, the transverse bending frequency and longitudinal frequency were calculated, and the FEA results show that structure's natural frequencies were almost unchanged. The strength of the structure was verified through two critical load cases. The lightweight supports of the dampers were designed and optimized. The final weight increment meets the engineering requirements.

Based on the design results, the damping system prototype was manufactured and installed into the PAF, in which the vibration test was implemented. Compared with the original state, the damping state PAF had lower transmissibility on the resonance peaks. Among them, the axial acceleration peak transmissibility decreased by 36%, and the lateral acceleration peak transmissibility decreased by 35% and 12%, while the transmissibility of other frequency ranges remained unchanged. The fundamental frequency of the structure changed by less than 5%.

The test results coincide well with the theoretical analysis results. The effectiveness and feasibility of the parallel vibration isolation scheme were verified by the experiments.

Author Contributions: Conceptualization, S.C.; Data curation, Y.L.; Formal analysis, M.Y., Y.Z. and Y.L.; Funding acquisition, S.C. and Z.P.; Project administration, S.C. and Z.P.; Supervision, S.C.; Validation, M.Y. and Z.P.; Visualization, M.Y., Y.Z. and Y.L.; Writing—original draft, Z.Y. and M.Y.; Writing—review & editing, S.C. and Z.Y. All authors have read and agreed to the published version of the manuscript.

Funding: This work was supported by the National Natural Science Foundation of China; Grant Number: 11672016.

Conflicts of Interest: The authors declare no conflict of interest.

References

1. Ma, X.R.; Han, Z.Y.; Zou, Y.J.; Ding, J.F. Review and Assessment of Spacecraft Mechanical Environment Analysis and Specification Determination. *J. Astronaut.* **2012**, *33*, 1–12.
2. Liu, C.; Jing, X.; Daley, S.; Li, F. Recent advances in micro-vibration isolation. *Tetrahedron Asymmetry* **2015**, *56*, 55–80. [CrossRef]
3. Wang, Z.; Jia, Y.; Xu, S.; Tang, L. Active vibration suppression in flexible spacecraft with optical measurement. *Aerosp. Sci. Technol.* **2016**, *55*, 49–56. [CrossRef]
4. Ma, X.R.; Han, Z.Y. *Analytical Methods and Test Techniques of Satellite and Launch Vehicle Mechanical Environment*; Science Press: Beijing, China, 2017; p. 392.
5. Wang, X.; Yu, Z.; Zhang, B.; Zhang, Q.; Pan, H. Progress of POGO suppression technology of launch vehicles at home and abroad. *Sci. Sin.* **2014**, *44*, 492–503. [CrossRef]
6. Johnson, C.D.; Wilke, P.S. Protecting Satellites from the Dynamics of the Launch Environment. In Proceedings of the AIAA Space 2003 Conference & Exposition, Long Beach, CA, USA, 23–25 September 2003; p. 910.
7. Johnson, C.D.; Wilke, P.S.; Darling, K.R. Multi-axis whole-spacecraft vibration isolation for small launch vehicles. *Proc. SPIE Int. Soc. Opt. Eng.* **2001**, *4331*, 153–161.
8. Sciulli, D.; Griffin, S.F. Whole-Spacecraft Hybrid Isolation System for Launch Vehicles. U.S. Patent 6,135,390, 24 October 2000.
9. Ruebsamen, D.T. *Evolved Launch Vibration Evolved Launch Vibration Isolation System (ELVIS) Demonstration unit Test Results*; The Aerospace Corporation: El Segundo, California, USA, 2003.
10. Chen, Y.; Fang, B.; Yang, T.; Huang, W. Study of Whole-spacecraft Vibration Isolators Based on Reliability Method. *Chin. J. Aeronaut* **2009**, *22*, 153–159. [CrossRef]
11. Stabile, A.; Aglietti, G.; Richardson, G.; Smet, G. Design and verification of a negative resistance electromagnetic shunt damper for spacecraft micro-vibration. *J. Sound Vib.* **2017**, *386*, 38–49. [CrossRef]
12. Wei, Z.J.; Li, D.X.; Xu, R. Vibration Isolation Research on the Metal Rubber Damping Rod of Payload Attach Fitting. *Adv. Mater. Res.* **2012**, *391–392*, 467–473. [CrossRef]

13. Zhou, S.C.; Wang, H.; Gao, J.; Chen, J.; Di, W.B.; Liu, J.H.; Tang, G.A. Analysis for the principle of whole-spacecraft vibration isolation. *J. Astronaut.* **2008**, *6*, 1752–1755.
14. Liu, L.K.; Zheng, G.T.; Huang, W.H. Octo-strut vibration isolation platform and its application to whole spacecraft vibration isolation. *J. Sound Vib.* **2006**, *289*, 726–744. [CrossRef]
15. Zhang, Y.; Sheng, C.; Hu, Q.; Li, M.; Guo, Z.; Qi, R. Dynamic analysis and control application of vibration isolation system with magnetic suspension on satellites. *Aerosp. Sci. Technol.* **2018**, *75*, 99–114. [CrossRef]
16. Deng, C.; Mu, D.; Guo, J.; Xie, P. Reducing the negative effects of flywheel disturbance on space camera image quality using the vibration isolation method. *Front. Optoelectron.* **2017**, *10*, 80–88. [CrossRef]
17. Zhang, Y.W.; Fang, B.; Chen, Y. *Processing of Dynamic features analysis and reliability study of whole-spacecraft vibration isolation, 2010 3rd International Symposium on Systems and Control in Aeronautics and Astronautics, Harbin, 2010*; IEEE: Harbin, China, 2010.
18. Du, H. Vibration Suppression of a Conical Honeycomb Satellite Adapter Subjected to Constrained Layer Damping. *Chin. J. Appl. Mech.* **2003**, *3*, 5–9+155.
19. Du, H.; Zou, Z.; Huang, W. Vibration suppression analysis for supporter with constrained layer damping. *J. Harbin Inst. Technol.* **2004**, *02*, 231–236.
20. Zhang, J.X.; Zhang, H.S.; Cao, X.R.; Zhang, H.J.; Wei, X.B. Constrained damping layer design and vibration suppression verification for vehicle instrument installation board. *Spacecr. Environ. Eng.* **2016**, *33*, 540–544.
21. Tu, F.C. Semi-Active Whole Spacecraft Vibration Isolation Technology Using Magnetorheological Damper. Ph.D. Thesis, Harbin Institute of Technology, Harbin, China, 2010.
22. Fei, H.; Song, E.; Ma, X.; Jiang, D. Research on whole-spacecraft vibration isolation based on parallel load-bearing and damping system. *Chin. J. Theor. Appl. Mech.* **2019**, *16*, 467–476.
23. Liu, L.K.; Zheng, G.T. Parameter analysis of PAF for whole-spacecraft vibration isolation. *Aerosp. Sci. Technol.* **2007**, *11*, 464–472. [CrossRef]